Integrated Sensing and Backscatter Communication

Diluka Galappaththige, *Member, IEEE*, Chintha Tellambura, *Fellow, IEEE,* Amine Maaref, *Senior Member, IEEE*

***Abstract*—Researchers are challenging the traditional approach to network design by exploring the integration of communication and sensing capabilities. In line with this trend, we present an innovative system called the Integrated Sensing and Backscatter Communication (ISABC) system and evaluate its performance. This system comprises a full-duplex base station (BS), a backscatter tag, and a user. The tag reflects the BS transmitted signal and provides data to the user. The BS extracts environmental information from the same signal. We provide closed-form expressions for the user and tag communication rates, as well as the sensing rate at the BS. Our study also offers comprehensive numerical performance results and simulation examples. We specifically investigate the impact of BS power allocation on communication and sensing. For example, a communication rate of $11.30\,\mathrm{bps/Hz}$ at the user and a sensing rate of $3.63\,\mathrm{bps/Hz}$ at the BS are possible with $20\,\mathrm{dBm}$ and $60\,\%$ power split. Our work provides valuable insights into the potential of ISABC systems and highlights the importance of optimizing their performance through power allocation.**

***Index Terms*—Backscatter communication (BackCom), Integrated sensing and communication (ISAC), Passive tags.**

I. Introduction

The integrated sensing and communication (ISAC) paradigm is a key enabler of beyond 5G/6G networks, offering significant benefits such as enhanced spectral efficiency, reduced hardware costs, and minimized electromagnetic pollution [1], [2]. Unlike traditional networks focused solely on communication, ISAC performs both sensing and communication functions simultaneously within the same time-frequency resource block. This allows ISAC nodes (Fig. 1a) to extract environmental information from received radio frequency (RF) signals and reflections, enabling new services like high-accuracy localization, gesture capturing, activity recognition, object detection, and tracking, as well as imaging and environment reconstruction [1], [2]. Additionally, the communication performance benefits from more accurate beamforming, faster beam failure recovery, and reduced channel estimation overhead.

Backscatter communication (BackCom) is emerging as a key candidate for supporting passive IoT networks, attracting the interest of both academia and industry [3]–[6]. Backscatter tags leverage RF signals generated by a source (either dedicated or ambient) to send their data to a reader (either dedicated or cooperative) [3]–[6]. They are thus inexpensive and have extremely-low energy requirements (a few nW-$\mu\mathrm{W}$) [3]. This improves spectrum utilization by avoiding the need for new spectrum allocations. In ambient BackCom (AmBC), legacy signals can directly interfere, limiting backscatter performance. However, the cooperative receiver/user can decode both primary and backscatter data, reducing primary interference to the BackCom system [7].

D. Galappaththige and C. Tellambura with the Department of Electrical and Computer Engineering, University of Alberta, Edmonton, AB, T6G 1H9, Canada (e-mail: {diluka.lg, ct4}@ualberta.ca).

A. Maaref is with Huawei Canada, 303 Terry Fox Drive, Suite 400, Ottawa, Ontario K2K 3J1 (e-mail: amine.maaref@huawei.com).

TABLE I: A comparison between ISAC and ISABC.

	ISAC	ISABC
Target	✓	✗
Tag	✗	✓
Additional data at the user	✗	✓
Power allocation at the BS	✓	✓
User decoding	Conventional	SIC

Building on both of these, we propose an innovative approach called Integrated Sensing and Backscatter Communications (ISABC), replacing the conventional sensing/radar target in ISAC systems with a passive tag (Fig. 1). ISAC and ISABC systems differ in several key aspects (Table I). First, the backscatter tag serves as the sensing target, providing sensing information to the base station (BS) while simultaneously transmitting additional data to the user. For example, the tag could be a sensor that transmits background information to the user, which allows the BS to use it as well to obtain environmental information, such as range, velocity, or angle. Second, by utilizing both sensing and backscatter data, ISABC systems significantly enhance communication and sensing performance, but the user's complexity increases due to the need for successive interference cancellation (SIC)-based decoding.

While conventional ISAC and BackCom systems have been extensively studied in isolation [3]–[11], the integration of these two technologies and its performance implications have remained unexplored until now. This letter presents the first investigation into their combined operation. As such, its primary contributions lie in merging BackCom with sensing and leveraging the tag's backscattered signal, which is unintentionally received by both the user and the BS, for sensing purposes.

This paper aims to integrate sensing capabilities with communications and quantify the benefits of ISABC systems. To achieve this, we examine an AmBC system consisting of a tag, a cooperative user, and a full-duplex (FD) BS (Fig. 1b). The FD BS can facilitate both user and tag communication, with the tag reflecting the BS's signal for data communication and the BS extracting environmental data from the reflected signal. In this study, we derive the closed-form ergodic communication rate and maximal sensing rate. We also explore the impact of power allocation at the BS on communication (user and tag) and sensing rates, using simulation examples. Our findings support the notion that ISABC systems have the potential to enhance spectral efficiency while providing additional information to the BS, resulting in improved communication and sensing performance.

Notation: Symbols $\mathbf{A}^{\mathrm{T}}$, $\mathbf{A}^{\mathrm{H}}$, $\mathbb{E}\{\cdot\}$, $\mathrm{Tr}(\cdot)$, and $\det(\cdot)$ denote transpose, Hermitian transpose, expected value, trace operator, and determinant operator, respectively. Further, complex Gaus-

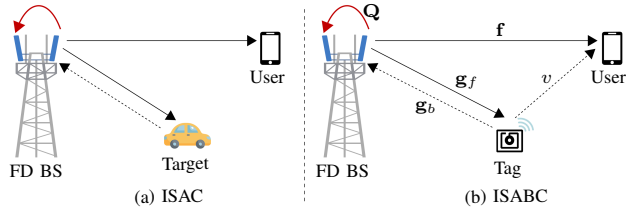

Fig. 1: Conventional ISAC and proposed ISABC system setups.

sian vector $\mathcal{CN}(\boldsymbol{\mu}, \mathbf{R})$ has mean $\boldsymbol{\mu}$ and co-variance matrix $\mathbf{R}$. Finally, $\mathcal{M} = \{1, \ldots, M\}$.

II. System, Channel, and Signal Models

A. System and Channel Models

We consider an ISABC network having an FD BS with $M \geq 1$ transmit and $N \geq 1$ receiver antennas, a single-antenna tag, and a single-antenna user (Fig. 1). The FD BS uses transmit beamforming to communicate with the user (and the tag) while broadcasting a sensing waveform. The tag utilizes that signal to send its data to the user. We assume a cooperative user who first decodes its data and then performs SIC to decode the tag's data. The FD BS uses the received backscatter signal to extract environmental information [8], [9], [12]. To mitigate the self-interference (SI), we assume that the BS has two sets of spatially well-separated antennas [8], [9], [12]. For simplicity, we thus assume perfect SI cancellation [8], [9], [12] and time synchronization among the nodes.

The channels between the BS and the user, the BS and the tag, and the tag and the user are denoted by $\mathbf{f} \in \mathbb{C}^{M\times 1}$, $\mathbf{g}_f \in \mathbb{C}^{M\times 1}$, and $v \in \mathbb{C}$, respectively. Moreover, $\mathbf{g}_b \in \mathbb{C}^{N\times 1}$ represents the channel between the tag and the FD BS receiver antennas. All these channels are modeled as Rayleigh fading, i.e., $\mathbf{a} \sim \mathcal{CN}(\mathbf{0}, \zeta_a \mathbf{I}_K)$, where $\mathbf{a} \in \{\mathbf{f}, \mathbf{g}_f, v, \mathbf{g}_b\}$, $K \in \{M, N, 1\}$, and ζ_a captures the large-scale path-loss and shadowing, which stays constant for several coherence intervals. Finally, the SI channel between the transmitter and the receiver of the BS is denoted as $\mathbf{Q} \in \mathbb{C}^{M\times N}$.

B. Signal Model

Comprising both data and sensing waveforms, the BS transmitted signal at the lth time slot, $\mathbf{x}(l) \in \mathbb{C}^{M\times 1}$, is given by

$$\mathbf{x}(l) = \sqrt{\rho p_t}\mathbf{w}x_d(l) + \sqrt{(1-\rho)p_t}\mathbf{s}(l), \tag{1}$$

where p_t is the transmit power, $x_d(l)$ is the data for the user, $\mathbf{w} \in \mathbb{C}^{M\times 1}$ is the beamforming vector of the BS, and $\mathbf{s}(l) \in \mathbb{C}^{M\times 1}$ is the sensing signal. All these three signals satisfy the standard energy normalization $\mathbb{E}\{\|\mathbf{x}\|^2\} = 1$. And ρ is the power allocation factor between communication and sensing.

The received signal at the user is given as

$$y(l) = \mathbf{f}^{\mathrm{H}}\mathbf{x}(l) + \sqrt{\alpha}\mathbf{h}^{\mathrm{H}}\mathbf{x}(l)c(l) + z_u(l), \tag{2}$$

where the first and second terms in (2) denote the direct-link and the backscatter link signals, $z_u(l) \sim \mathcal{CN}(0, \sigma^2)$ is the additive white Gaussian noise (AWGN) at the user. Moreover, in (2), $\mathbf{h}$ is the effective backscatter channel through the tag, i.e., $\mathbf{h} = \mathbf{g}_f v$, α is the tag's reflection coefficient satisfying $0 \leq \alpha \leq 1$, and $c(l)$ is the tag's data with $\mathbb{E}\{|c(l)|^2\} = 1$. We assume that the sensing waveform is designed using only the communication channel statistics [10], [11]. Therefore, the user knows the transmitted sensing waveform in advance and removes it before decoding its data. Thus, after the sensing signal removal, the received signal may be expressed as

$$\begin{aligned} y'(l) = &\sqrt{\rho p_t}\mathbf{f}^{\mathrm{H}}\mathbf{w}x_d(l) + \sqrt{\alpha\rho p_t}\mathbf{h}^{\mathrm{H}}\mathbf{w}x_d(l)c(l) \\ &+\sqrt{\alpha(1-\rho)p_t}\mathbf{h}^{\mathrm{H}}\mathbf{s}(l)c(l) + z_u(l). \end{aligned} \tag{3}$$

Next, to recover the data from the tag, the user performs SIC decoding. That is, the user initially decodes its own signal while treating tag signals as interference. The user then subtracts the decoded signal $x_d(l)$ from $y'(l)$ and performs SIC decoding of the tag signal. To this end, the signal following the SIC decoding of the tag's data at the user is given as

$$\begin{aligned} y_t(l) = &\sqrt{\alpha\rho p_t}\mathbf{h}^{\mathrm{H}}\mathbf{w}x_d(l)c(l) \\ &+\sqrt{\alpha(1-\rho)p_t}\mathbf{h}^{\mathrm{H}}\mathbf{s}(l)c(l) + z_u(l). \end{aligned} \tag{4}$$

The backscattered signal at the tag is received not only by the users but also by the BS. It aims to extract environmental information from this signal. The received signal at the FD BS at the lth time slot, $\mathbf{y}_b(l) \in \mathbb{C}^{N\times 1}$, is thus given as

$$\mathbf{y}_b(l) = \sqrt{\alpha}\mathbf{G}^{\mathrm{H}}\mathbf{x}(l)c(l) + \mathbf{Q}^{\mathrm{H}}\mathbf{x}(l) + \mathbf{z}_b(l), \tag{5}$$

where $\mathbf{z}_b(l) \sim \mathcal{CN}(\mathbf{0}, \sigma^2\mathbf{I}_N)$ is the AWGN at the FD BS. Besides, $\mathbf{G} = \mathbf{g}_f\mathbf{g}_b^{\mathrm{H}} = [\mathbf{g}_1, \ldots, \mathbf{g}_N] \in \mathbb{C}^{M\times N}$ is the target sensing response matrix of the tag, which contains the environmental information [10], [11]. Besides, $\mathbf{g}_n = \mathbf{g}_f[\mathbf{g}_b]_n$, where $[\mathbf{g}_b]_n$ is the nth element of $\mathbf{g}_b$. We assume that the FD BS cancels the SI at its receiver using perfect SI cancellation techniques [8], [9], [12]. To this end, the post-processed SI canceled signal at the BS is given as

$$\mathbf{y}'_b(l) = \sqrt{\alpha p_t}\mathbf{G}^{\mathrm{H}}\left(\sqrt{\rho}\mathbf{w}x_d(l) + \sqrt{1-\rho}\mathbf{s}(l)\right)c(l) + \mathbf{z}_b(l). \tag{6}$$

The BS collects signals over L time slots to extract the sensing information [10], [11]. Thus, it exploits the following signal:

$$\begin{aligned} \mathbf{Y}_b &= \sqrt{\alpha p_t}\mathbf{G}^{\mathrm{H}}(\mathbf{S} + \mathbf{X}_d) + \mathbf{Z}_b \\ &= \sqrt{\alpha p_t}\mathbf{G}^{\mathrm{H}}\mathbf{S} + \mathbf{Z}, \quad \in \mathbb{C}^{N\times L}, \end{aligned} \tag{7}$$

where $\mathbf{S} = \sqrt{1-\rho}[\mathbf{s}(1)c(1), \ldots, \mathbf{s}(L)c(L)] \in \mathbb{C}^{M\times L}$, $\mathbf{X}_d = \sqrt{\rho}\mathbf{w}[x_d(1)c(1), \ldots x_d(L)c(L)]\mathbb{C}^{M\times L}$, and $\mathbf{Z}_b = [\mathbf{z}_b(1), \ldots, \mathbf{z}_b(L)] \in \mathbb{C}^{M\times L}$. Moreover, $\mathbf{Z} = \sqrt{\alpha p_t}\mathbf{G}^{\mathrm{H}}\mathbf{X}_d + \mathbf{Z}_b$ is the aggregated/effective interference-plus-noise and treated as the Gaussian noise [10], [11]. Note that the received sensing signal at the FD BS, $\mathbf{s}(l)$, contains unknown backscatter data, $c(l)$. Hence, we assume that a small portion of coherence time is allocated for uplink transmission in each coherence interval following downlink transmission. In particular, during this time, the tag remains silent, and the user transmits the decoded tag's data to the FD BS. Thereby, the BS can estimate the unknown backscatter signal and remove its effect from the received sensing signal[1].

III. Performance Analysis

In this section, we analyze the user's communication performance and BS's sensing performance.

[1]Here, the uplink is assumed perfect and omitted. However, the effects of uplink transmission and other impairments will be addressed in future work.

A. Communication Performance

The tag and user communication performance is specified by the achieved data rate. We focus on the lth time slot.

1) The User Rate: Using (3), the received signal-to-interference-plus-noise ratio (SINR) is obtained as

$$\gamma_u' = \frac{\rho p_t |\mathbf{f}^{\mathrm{H}}\mathbf{w}|^2}{\alpha\rho p_t |\mathbf{h}^{\mathrm{H}}\mathbf{w}|^2 + \alpha(1-\rho)p_t\|\mathbf{h}\|^2 + \sigma^2}. \tag{8}$$

The achievable rate of the user data is thus given as

$$\mathcal{R}_u = \mathbb{E}_{\mathbf{a}}\{\log_2(1+\gamma_u')\} \text{ bps/Hz}. \tag{9}$$

To derive a closed-form solution, we invoke [13, *Lemma 1*]. The rate is thus approximated as

$$\mathcal{R}_u \approx \log_2(1+\gamma_u) \text{ bps/Hz}, \tag{10}$$

where γ_u is given as

$$\gamma_u = \frac{\rho p_t \mathbb{E}\{|\mathbf{f}^{\mathrm{H}}\mathbf{w}|^2\}}{\alpha\rho p_t \mathbb{E}\{|\mathbf{h}^{\mathrm{H}}\mathbf{w}|^2\} + \alpha(1-\rho)p_t\mathbb{E}\{\|\mathbf{h}\|^2\} + \sigma^2}. \tag{11}$$

We assume the FD BS adopts weighted MRT beamforming to transmit data toward the user and energy toward the tag. To this end, the FD BS's beamforming vector is given as $\mathbf{w} = (\mu\mathbf{f} + (1-\mu)\mathbf{g}_f)/\sqrt{\psi}$, where ψ is the normalization factor, i.e., $\psi = \mathbb{E}\{\|\mu\mathbf{f} + (1-\mu)\mathbf{g}_f\|^2\} = \mu^2 M\zeta_f + (1-\mu)^2 M\zeta_{g_f}$, and μ is the weight factor. Hence, the closed-form of the user SINR (11) is given as (12), where $\zeta_h = \zeta_v\zeta_{g_f}$ (Appendix A).

2) The Tag Rate: Following a similar approach to the user rate and using (4), the tag's rate is approximated as

$$\mathcal{R}_t \approx \mathbb{E}_{x_d}\{\log_2(1+\gamma_t)\} \text{ bps/Hz}, \tag{13}$$

where γ_t is given as

$$\gamma_t = \frac{\alpha\rho p_t}{\sigma^2}\mathbb{E}\{|\mathbf{h}^{\mathrm{H}}\mathbf{w}|^2\}|x_d(l)|^2 + \frac{\alpha(1-\rho)p_t}{\sigma^2}\mathbb{E}\{\|\mathbf{h}\|^2\}. \tag{14}$$

Next, by evaluating the expectation terms in (14), the closed-form of the tag's SINR is given as (15). Assuming the squared envelope of $x_d(l)$ follows an exponential distribution, i.e., $f_{x_d}(x) = e^{-x}$ for $x > 0$, the tag's rate is derived by taking the expectation over $x_d(l)$ as follows:

$$\mathcal{R}_t \approx \log_2(e)\left(\ln(b_t+1) - \mathrm{E}_i\left(\frac{-(b_t+1)}{a_t}\right)e^{\frac{b_t}{a_t}+\frac{1}{a_t}}\right), \tag{16}$$

where

$$a_t \triangleq \frac{\alpha\rho p_t}{\psi\sigma^2}\left(\mu^2 M\zeta_h\zeta_f + (1-\mu)^2 M(M+1)\zeta_h\zeta_{g_f}\right), \tag{17a}$$

$$b_t \triangleq \frac{\alpha(1-\rho)p_t}{\sigma^2}M\zeta_h. \tag{17b}$$

Additionally, $\mathrm{E}_i(x) = \int_{-\infty}^{x} u^{-1}e^u du$ is the exponential integral function. Note that, $-e^{\frac{1}{x}}\mathrm{E}_i(-1/x)$ is monotonically increasing and concave function of x [14].

Remark 1. *The received signal power at the tag is given as*

$$P_r^{\mathrm{tag}}(l) = |\mathbf{g}_f^{\mathrm{H}}\mathbf{x}(l)|^2 = \left|\mathbf{g}_f^{\mathrm{H}}\left(\sqrt{\rho p_t}\mathbf{w}x_d(l) + \sqrt{(1-\rho)p_t}\mathbf{s}(l)\right)\right|^2. \tag{18}$$

Since $\mathbf{w}$ *and* $\mathbf{s}(l)$ *satisfy* $\mathbb{E}\{\|\mathbf{w}\|^2\} = 1$ *and* $\mathbb{E}\{\|\mathbf{s}(l)\|^2\} = 1$*, respectively, the received signal power or the reflected/backscattered power at the tag does not depend on the power allocation at the FD BS. The tag's performance solely depends on the total transmit power and its reflection coefficient. This will be also reflected in the simulation examples.*

B. Sensing Performance

The BS uses the received signal (7) to sense the target sensing response $\mathbf{G}$. To this end, sensing performance is assessed using sensing rate, defined as sensing mutual information (MI) per unit-time [12]. Specifically, the sensing MI is the MI between the received signal at the BS, $\mathbf{Y}_b$, and the sensing target response, $\mathbf{G}$, for a given $\mathbf{S}$ [12].

To evaluate the sensing rate, under the considered model, we have $\mathbf{g}_n \sim \mathcal{CN}(\mathbf{0}, \mathbf{R}_g)$, where $\mathbf{R}_g \triangleq \mathbb{E}\{\mathbf{g}_n\mathbf{g}_n^{\mathrm{H}}\} \succ \mathbf{0}$ is the transmit correlation matrix, $\mathbb{E}\{\mathbf{g}_n\mathbf{g}_{n'}^{\mathrm{H}}\} = \mathbf{0}$ for $n \neq n'$, and $\mathbb{E}\{\mathbf{z}_b(l)\mathbf{z}_b(l')^{\mathrm{H}}\} = \mathbf{0}$ for $l \neq l'$. Hence, the sensing rate implies the following [12]:

1) The sensing rate indicates how much environmental information can be extracted from $\mathbf{Y}_b$.
2) In estimating $\mathbf{G}$, the optimal sensing waveform based on maximizing the sensing rate has the same estimation performance as the optimal sensing waveform based on minimizing the mean-square error (MSE).

Assuming that each sensing waveform symbol lasts one unit time, the sensing MI is given as

$$\mathcal{I} = \frac{1}{L}I(\mathbf{Y}_b; \mathbf{G}|\mathbf{S}), \tag{19}$$

where $I(X;Y|Z)$ is the MI between X and Y conditioned on Z. Because the effective/aggregate interference-plus-noise, $\mathbf{Z}$, is treated as Gaussian noise, it yields a sensing performance lower bound in the worst-case design perspective [15]. Besides, we have $\mathbf{x}_d(l) \sim \mathcal{CN}(\mathbf{0}, \mathbf{R}_x)$, where $\mathbf{R}_x \triangleq \mathbb{E}\{\mathbf{x}_d(l)\mathbf{x}_d(l)^{\mathrm{H}}\} = \rho/\psi\mathbb{E}\{\mathbf{w}\mathbf{w}^{\mathrm{H}}\}$, and $\mathbb{E}\{\mathbf{x}_d(l)\mathbf{x}_d(l')^{\mathrm{H}}\} = \mathbf{0}$ for $l \neq l'$. To characterize the sensing MI in closed-form, we invoke [10, *Lemma 1*] and the sensing MI is thus given as

$$\mathcal{I} = \frac{N}{L}\log_2\left(\det\left(\mathbf{I}_L + \frac{\alpha(1-\rho)p_t}{\sigma_z^2}\mathbf{S}^{\mathrm{H}}\mathbf{R}_g\mathbf{S}\right)\right), \tag{20}$$

where $\sigma_z^2 = \sigma^2 + \mathrm{Tr}\,(\mathbf{R}_g\mathbf{R}_x)$. From (20) and the definition of the sensing rate, the maximal sensing rate is derived as

$$\mathcal{R}_s = \underset{\mathrm{Tr}(\mathbf{S}\mathbf{S}^{\mathrm{H}})\leq 1}{\text{maximize}} \quad \mathcal{I} = \frac{N}{L}\sum_{m\in\mathcal{M}}\log_2\left(1 + \frac{\alpha(1-\rho)p_t}{\sigma_z^2}\lambda_m s_m^\star\right) \text{ bps/Hz}, \tag{21}$$

where $\lambda_m > 0$ for $m \in \mathcal{M}$ denotes the mth eigenvalue of $\mathbf{R}_g$ and $s_m^\star = \max\{0, 1/v - \sigma_z^2/\lambda_m\}$ with $\sum_{m\in\mathcal{M}}\max\{0, 1/v - \sigma_z^2/\lambda_m\} = 1$ [10].

IV. Simulation Results

This section presents simulations of both communications (i.e., direct and backscatter) and sensing performance. We model large-scale fading, ζ_a, with the carrier frequency f_c using the 3GPP UMi model [16, Table B.1.2.1], and the

$$\gamma_u = \frac{\rho p_t \left(\mu^2 M(M+1)\zeta_f^2 + (1-\mu)^2 M \zeta_f \zeta_{g_f}\right)/\psi}{\alpha\rho p_t \left(\mu^2 M \zeta_f \zeta_h + (1-\mu)^2 M(M+1)\zeta_h \zeta_{g_f}\right)/\psi + \alpha(1-\rho)p_t M \zeta_h + \sigma^2} \tag{12}$$

$$\gamma_t = \frac{\alpha\rho p_t}{\psi\sigma^2}\left(\mu^2 M \zeta_h \zeta_f + (1-\mu)^2 M(M+1)\zeta_h \zeta_{g_f}\right)|x_d(l)|^2 + \frac{\alpha(1-\rho)p_t}{\sigma^2} M \zeta_h \tag{15}$$

TABLE II: Simulation settings

Parameter	Value	Parameter	Value
f_c	3 GHz	d_f	15 m
B	10 MHz	$d_{g_f} = d_{g_b}$	6 m
N_f	10 dB	d_v	10 m
α	0.6	$M = N$	16
μ	0.5	L	5

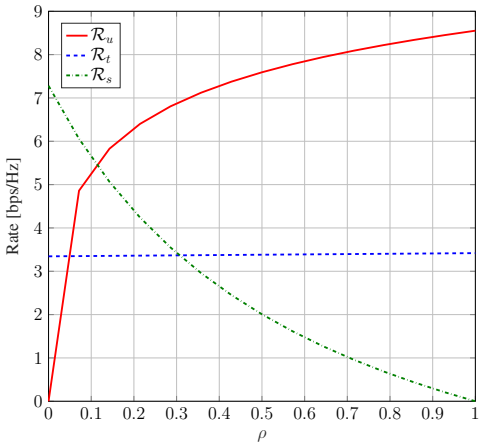

Fig. 2: Communication and sensing rate as a function of ρ for $p_t = 20\,\text{dBm}$.

AWGN variance as $\sigma^2 = 10\log_{10}(N_0 B N_f)$ dBm, where $N_0 = -174\,\text{dBm/Hz}$, B is the bandwidth, and N_f is the noise figure. Unless otherwise specified, Table II provides the simulation parameters.

As a comparative benchmark, we consider the conventional ISAC system (Fig. 1a) as follows: (i) the communication performance without the backscatter tag, i.e., $\alpha = 0$ in (8), and (ii) the sensing performance with no reflection loss at the target, i.e., $\alpha = 1$ in (20).

Fig. 2 investigates the effect of BS power allocation on the communication and sensing rates. To this end, we plot the user rate, $\mathcal{R}_u$ (10), tag rate, $\mathcal{R}_t$ (16), and sensing rate, $\mathcal{R}_s$ (21), as functions of power allocation coefficient, ρ, for p_t =20 dBm. When $\rho = 0$, the BS transmits the sensing signal only. Hence, the user data rate drops to zero. However, the tag's rate at the user is independent of ρ. For fixed α and p_t, the tag rate is thus a constant. For $\rho = 0$, the sensing rate is maximized because the total transmit power is allocated for sensing. Similarly, as $\rho \to 1$, the user achieves the highest data rate while the sensing rate reaches zero. Hence, these rate curves for a given ρ yield the achievable trade-offs between communications and sensing performance. Based on application-specific minimum rate requirements, one can select ρ from Fig. 2.

Fig. 3 plots the user and communication rates against the BS transmit power for $\rho = \{0.4, 0.6, 0.8\}$. In Fig. 3, (10) and (16) are used to plot the user and tag rates, and their accuracy is validated using Monte-Carlo simulation. As expected, the tag rate is independent of ρ, while a high ρ contributes to a higher user rate. For instance, with the BS at 20 dBm, a user

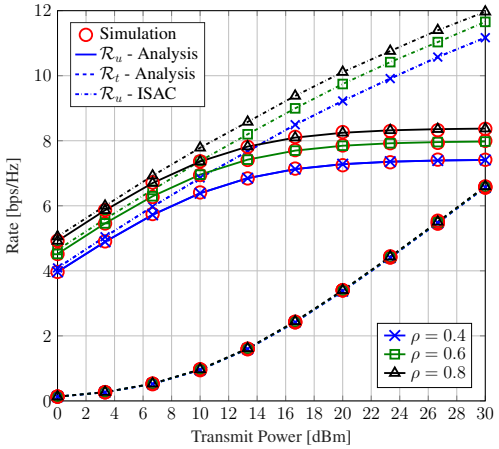

Fig. 3: Communication rate versus transmit power for $\rho = \{0.4, 0.6, 0.8\}$.

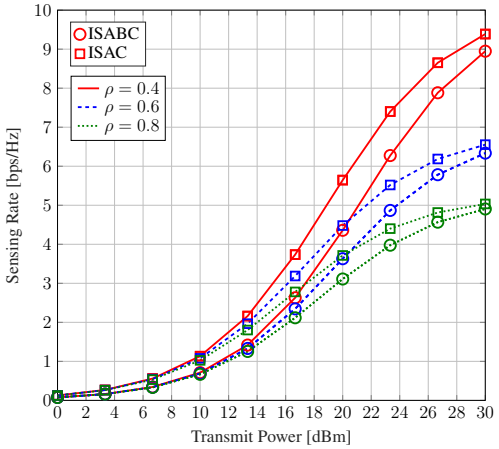

Fig. 4: Sensing rate versus transmit power for $\rho = \{0.4, 0.6, 0.8\}$.

rate increases 13.3 % when ρ from 0.4 and 0.6. However, due to the absence of tag interference, the ISAC benchmark user rate is always higher than the proposed ISABC user rate.

Fig. 4 depicts the BS's sensing rate versus the transmit power. Three sets of curves are plotted by varying power allocation, i.e., $\rho = \{0.4, 0.6, 0.8\}$. As expected, increasing the transmit power improves the sensing rate of the BS, because of the higher reflected power from the tag. Furthermore, low ρ values result in a high sensing rate due to the high power allocation for the sensing waveform. For example, $\rho = 0.4$ achieves a 66.7 % sensing rate gain than that of $\rho = 0.8$ due to the allocated high power for sensing. Moreover, the ISAC system achieves higher sensing rates than the ISABC system as there is no reflection loss at the target.

Nevertheless, the proposed system outperforms ISAC. For example, the ISABC system delivers a 15 % sum rate gain, i.e., $\mathcal{R}_u + \mathcal{R}_t + \mathcal{R}_s$, at 30 dBm and $\rho = 0.6$.

In Fig. 5, we characterize the communication (user)-sensing rate region for different transmit power levels at the BS, i.e., $p_t = \{10, 15, 18, 20\}$ dBm. In particular, the rate region is

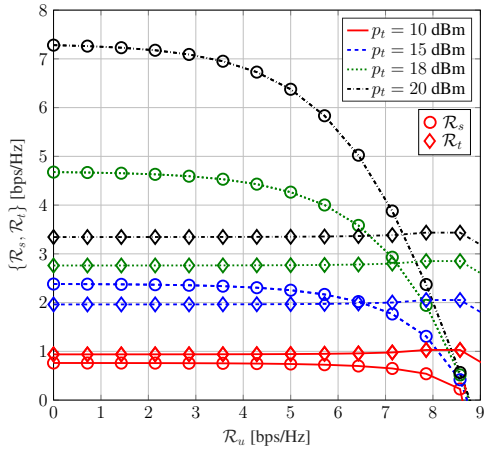

Fig. 5: Rate region for $p_t = \{10, 15, 18, 20\}$ dBm.

plotted by commuting the power allocation coefficient at the BS for a given user rate and then allocating the remaining transmit power for the sensing signal. We also plot the tag rate to observe the effect on the BackCom. As shown in Fig. 5, when there is no communication rate requirement, the sensing rate achieves its highest values based on the transmit power. In contrast, the user demanding a non-zero rate requirement adversely affects the sensing rate as more power is allocated for communication. As previously observed, the tag rate is unaffected by the user rate or the sensing rate, i.e., power allocation at the BS. It solely depends on the total transmit power and the tag's reflection coefficient.

V. Conclusion

In this letter, we present a novel approach that integrates sensing with a passive tag, distinguishing it from the standard ISAC where the BS senses a random target. In our system, the BS senses the signal reflected by the tag to extract valuable environmental information. We carefully analyze the communication performance of both the primary user and the backscatter tag, as well as the sensing performance at the BS.

Through our analysis, we discovered that power allocation at the BS plays a pivotal role in influencing user and sensing rates, but it surprisingly has no effect on the backscatter rate. This observation highlights the unique nature of our proposed integration, where environmental information extraction is achieved without affecting the backscatter communication performance. This innovative concept opens up new possibilities for leveraging passive tags as active participants in environmental monitoring and wireless communication systems. Future works include the optimal power allocation at the BS, multi-tag and multi-user configurations with integrated sensing, and interference mitigation techniques.

Appendix A
Derivation of γ_u in (12)

We begin by first computing the expectation term in the numerator of (11) as follows:

$$\begin{aligned}\mathbb{E}\{|\mathbf{f}^{\mathrm{H}}\mathbf{w}|^2\} &= \mathbb{E}\{|\mathbf{f}^{\mathrm{H}}\left(\mu\mathbf{f} + (1-\mu)\mathbf{g}_f\right)|^2\} \\ &= \mu^2\mathbb{E}\{|\mathbf{f}^{\mathrm{H}}\mathbf{f}|^2\} + (1-\mu)^2\mathbb{E}\{|\mathbf{f}^{\mathrm{H}}\mathbf{g}_f|^2\} \\ &\overset{(a)}{=} \mu^2 M(M+1)\zeta_f^2 + (1-\mu)^2 M\zeta_f\zeta_{g_f}, \quad (22)\end{aligned}$$

where (a) is evaluated from the fact that, for any vector $\mathbf{z} \sim \mathcal{CN}(\mathbf{0}, \theta\mathbf{I}_M)$, we have $\mathbb{E}\left\{|\mathbf{z}^{\mathrm{H}}\mathbf{z}|^2\right\} = (M^2+M)\theta^2$ [17].

Next, the first expectation term in the denominator of (11) is

$$\begin{aligned}\mathbb{E}\{|\mathbf{h}^{\mathrm{H}}\mathbf{w}|^2\} &= \mathbb{E}\{|\mathbf{h}^{\mathrm{H}}\left(\mu\mathbf{f} + (1-\mu)\mathbf{g}_f\right)|^2\} \\ &= \mu^2\mathbb{E}\{|\mathbf{h}^{\mathrm{H}}\mathbf{f}|^2\} + (1-\mu)^2\mathbb{E}\{|v\mathbf{g}_f^{\mathrm{H}}\mathbf{g}_f|^2\} \\ &= \mu^2 M\zeta_f\zeta_h + (1-\mu)^2 M(M+1)\zeta_h\zeta_{g_f}. \quad (23)\end{aligned}$$

The second expectation in the denominator of (11) is

$$\mathbb{E}\{\|\mathbf{h}\|^2\} = \mathbb{E}\{\mathbf{h}^{\mathrm{H}}\mathbf{h}\} = \mathbb{E}\{v\mathbf{g}_f^{\mathrm{H}}\mathbf{g}_f v\} = M\zeta_h. \quad (24)$$

By substituting (22), (23), and (24) into (11), the closed-form SINR of the user is derived as in (12).

References

[1] J. A. Zhang *et al.*, "Enabling joint communication and radar sensing in mobile networks — A survey," *IEEE Commun. Surveys Tuts.*, vol. 24, no. 1, pp. 306–345, 1st Quart. 2022.

[2] J. Wang *et al.*, "Integrated sensing and communication: Enabling techniques, applications, tools and data sets, standardization, and future directions," *IEEE Internet Things J.*, vol. 9, no. 23, pp. 23 416–23 440, Dec. 2022.

[3] D. T. Hoang, D. Niyato, D. I. Kim, N. V. Huynh, and S. Gong, *Ambient Backscatter Communication Networks*. Cambridge University Press, 2020.

[4] D. Galappaththige, F. Rezaei, C. Tellambura, and S. Herath, "Link budget analysis for backscatter-based passive IoT," *IEEE Access*, vol. 10, pp. 128 890–128 922, Dec. 2022.

[5] F. Rezaei, D. Galappaththige, C. Tellambura, and S. Herath, "Coding techniques for backscatter communications - A contemporary survey," *IEEE Commun. Surveys Tuts.*, vol. 25, no. 2, pp. 1020–1058, 2nd Quart. 2023.

[6] W. Liu, Y.-C. Liang, Y. Li, and B. Vucetic, "Backscatter multiplicative multiple-access systems: Fundamental limits and practical design," *IEEE Trans. Wireless Commun.*, vol. 17, no. 9, pp. 5713–5728, Sept. 2018.

[7] Y.-C. Liang, R. Long, Q. Zhang, and D. Niyato, "Symbiotic communications: Where Marconi meets Darwin," *IEEE Wireless Commun.*, vol. 29, no. 1, pp. 144–150, Feb. 2022.

[8] F. Liu, Y.-F. Liu, A. Li, C. Masouros, and Y. C. Eldar, "Cramér-Rao bound optimization for joint radar-communication beamforming," *IEEE Trans. Signal Process.*, vol. 70, pp. 240–253, Jan. 2022.

[9] M. L. Rahman, J. A. Zhang, X. Huang, Y. J. Guo, and R. W. Heath, "Framework for a perceptive mobile network using joint communication and radar sensing," *IEEE Trans. Aerosp. Electron. Syst.*, vol. 56, no. 3, pp. 1926–1941, Jun. 2020.

[10] C. Ouyang, Y. Liu, and H. Yang, "Performance of downlink and uplink integrated sensing and communications (ISAC) systems," *IEEE Wireless Commun. Lett.*, vol. 11, no. 9, pp. 1850–1854, Sept. 2022.

[11] ——, "On the performance of uplink ISAC systems," *IEEE Commun. Lett.*, vol. 26, no. 8, pp. 1769–1773, Aug. 2022.

[12] B. Tang and J. Li, "Spectrally constrained MIMO radar waveform design based on mutual information," *IEEE Trans. Signal Process.*, vol. 67, no. 3, pp. 821–834, Feb. 2019.

[13] Q. Zhang, S. Jin, K.-K. Wong, H. Zhu, and M. Matthaiou, "Power scaling of uplink massive MIMO systems with arbitrary-rank channel means," *IEEE J. Sel. Topics Signal Process.*, vol. 8, no. 5, pp. 966–981, 2014.

[14] R. Long, Y.-C. Liang, H. Guo, G. Yang, and R. Zhang, "Symbiotic radio: A new communication paradigm for passive internet of things," *IEEE Internet Things J.*, vol. 7, no. 2, pp. 1350–1363, Feb. 2020.

[15] B. Hassibi and B. Hochwald, "How much training is needed in multiple-antenna wireless links?" *IEEE Trans. Inf. Theory*, vol. 49, no. 4, pp. 951–963, Apr. 2003.

[16] "3GPP TR 36.814, further advancements for E-UTRA physical layer aspects, V.9.0.0 Rel. 9," Mar. 2010. Available Online: https://portal.3gpp.org/desktopmodules/Specifications/SpecificationDetails.aspx?specificationId=2493.

[17] A. M. Tulino and S. Verdu, *Random Matrix Theory and Wireless Communications*, Jan. 2004, vol. 1.